Journal of Applied Physics

Innovative non-thermal plasma coating for "core–shell" $CaCu_3Ti_4O_{12}$ material

Cite as: J. Appl. Phys. **130**, 163305 (2021); https://doi.org/10.1063/5.0061180
Submitted: 24 June 2021 • Accepted: 03 October 2021 • Published Online: 27 October 2021

Samir Merad, Daniela Maria Neacsa, Jean-Paul Rusiecki, et al.

AIP Publishing

Journal of Applied Physics ARTICLE scitation.org/journal/jap

Innovative non-thermal plasma coating for "core–shell" $CaCu_3Ti_4O_{12}$ material

Cite as: J. Appl. Phys. **130**, 163305 (2021); doi: 10.1063/5.0061180
Submitted: 24 June 2021 · Accepted: 3 October 2021 ·
Published Online: 27 October 2021

Samir Merad, Daniela Maria Neacsa, Jean-Paul Rusiecki, Sylvain Roger, François Gervais, Cécile Autret-Lambert, and Olivier Motret[a)]

AFFILIATIONS

GREMAN, UMR7347 CNRS, Université de Tours, Parc de Grandmont, F-37200 Tours, France

[a)]**Author to whom correspondence should be addressed:** olivier.motret@univ-tours.fr

ABSTRACT

Colossal permittivity of $CaCu_3Ti_4O_{12}$ (CCTO) makes it a very interesting candidate for capacitor applications. To improve its properties, an innovative physical method based on a pulsed non-thermal micro-plasma treatment was set up to realize the coating of CCTO's grains (core) with silicon oxide (shell). This method is adapted to control the thickness and homogeneity of the shell, which will allow a better control of grain–grain boundary interfaces and improve the properties of this material. Best result is obtained for the set of gas mixture: Ar/O_2/hexamethyldisiloxane (HMDSO) = 2028 N cm^3 min^{-1}/7.84 N cm^3 min^{-1}/523 mg h^{-1}, respectively, in plasma with a shell thickness of 50 nm. This study offers a new opportunity to quickly synthetize core–shell materials with a dry technique and without almost no secondary product resulting from the chemical reaction because it is in the gaseous state. A complete analysis of the plasma by optical emission spectroscopy in the UV-visible range shows that HMDSO molecules are totally dissociated in atomic (Si, C, and O) or simple radical species (C_2 and CH) in the plasma phase. In addition, several thermometer species (OH°, CH, CN, N_2, and N_2^+) are used to estimate excitation temperatures of the plasma (Trot, Tvib, and Te = 300 K, 2400–3700 K, and 5.3 eV, respectively) that clearly shows the non-equilibrium character and the efficiency of this plasma.

I. INTRODUCTION

In recent years, capacitors have invaded the electronics market through their use in all technological fields, such as automotive, home appliance, and aeronautical. It provides filtering or energy storage functions in electronic circuits. This strong demand has led to a great interest in dielectric materials with a high energy density. The expected characteristics for dielectrics-based solid-state capacitors are high permittivity ($\epsilon_r > 10^3$) and low dielectric loss ($\tan\delta < 10^{-1}$).[1] In traditional ferroelectric (FE) oxides, high permittivity is achieved due to their large dielectric response at the paraelectric (PE)–FE transition temperature.[2,3] The strong temperature dependence of the FE materials limits their applications. In order to achieve high performance for practical applications, an intensive research was focused on the dielectric materials that have nearly temperature and frequency-independent dielectric constants and small dielectric loss.[4,5] Since the beginning of this century, a new material with colossal permittivity was discovered, the perovskite-type material $CaCu_3Ti_4O_{12}$ (CCTO). CCTO exhibits a colossal dielectric constant $\epsilon_r \sim 10^4$ at low frequency, which remains almost constant between 100 and 600 K and slightly dependent on a large frequency in the 10^2–10^5 Hz range.[6–8]

Numerous investigations have revealed that the dielectric properties of CCTO strongly depend on the processing conditions during preparation, the type of external contacts, and the measuring frequency.[9,10] Many investigations have been performed to explain the origin of the giant dielectric constant for CCTO, which has been ambiguous until now.[11,12] It seems to be accepted that the giant dielectric constant is due to external effects, like the Internal Barrier Layer Capacitance (IBLC) model. This model is associated with an electrically heterogeneous microstructure consisting of semi-conducting grains and insulating grain boundaries.[13,14] It has been proved that the grain boundaries play an important role in the dielectric behavior.[15,16]

Unfortunately, this material exhibits a high dielectric loss ($\tan\delta > 0.05$ at 1 kHz) and conductivity despite its high dielectric constant. The dissipation factor is one important parameter for the application of a dielectric. Indeed, a material that has a high dielectric constant and a low loss factor is desirable in use as a capacitor

component. Then, the high loss tangent is still the most serious problem for applications based on capacitive components. To solve this problem and improve the CCTO properties, core–shell microstructure is one of the proposed solutions in the literature. The core–shell method consists of coating the grains with insulant materials like SiO_2, TiO_2, and Al_2O_3 to control the microstructure of the grain boundaries. It attempts normally to increase the resistivity and reduce the dielectric losses while keeping a high permittivity.[17] After sintering of the powder, the dielectric properties of the core–shell materials show promising results when compared to the CCTO ceramics but also to Grain Boundary Barrier Layer (GBBL) $SrTiO_3$-based capacitor.[18,19]

It, therefore, seems interesting to explore a new approach to coat CCTO grains with silicon oxides by cold plasma treatments. Cold plasmas, also named non-thermal plasmas, have shown their high efficiency in many industrial fields, including the abatement of gaseous and liquid hazardous species,[20–23] inactivation of micro-organisms in biomedical applications, food industry,[24–29] and surface interactions.[30–33]

During the last 20 years, new promising processes based on various micro-plasma configurations were investigated.[34–37] Micro-plasmas are characterized by a reduced size. One of the discharge dimensions must be sub-millimeter, corresponding to a value of $p \times d$ (pressure × discharge gap) between 1 and 13 Pa m close to those of low-pressure plasmas, but with pressures that can reach atmospheric pressure. Consequently, current and energy densities are much higher for conventional low-pressure plasmas. This leads to greater efficiency in the production of chemically active species in such plasmas.[38] These processes with small reaction volumes translate directly into very short processing times.

Plasma Enhanced Chemical Vapor Deposition (PECVD) technique was successfully used since many years for plasmas deposition processes. Classically, the plasma was generated by RF-excitation (at 13.56 MHz).[39–41] However, the coupling of a micro-plasma reactor with a nanosecond-pulsed electric generator can present many advantages: on one hand, this allows to benefit from the intrinsic properties of micro-plasmas and, on the other hand, the pulsed plasmas result in a very efficient energy transfer, i.e., input energy is mainly used to produce active species (hot electrons, free radicals, and ionic species) leading to chemical reactions but not to gas heating. Excitation temperature, i.e., rotational, vibrational, and electronic temperatures (Trot, Tvib, and Te), estimations are therefore very important to characterize the plasma reactivity. These parameters provide information notably on the input energy distribution and contribute to identify the main mechanisms responsible for chemical transformations into the plasma.

It could be interesting to prepare core–shell materials without wet surface treatment. We tried to set up a new physical method to realize the coating in order to control the thickness and homogeneity of the coating and with it the microstructure of the grain boundaries. Transmission electron microscopy (TEM) results confirm this "core–shell" microstructure for CCTO grains. The CCTO grains were covered with a SiO_2 shell which was produced by the decomposition of hexamethyldisiloxane (HMDSO) by an Ar/O_2 pulsed non-thermal plasma. HMDSO is a precursor frequently used in PECVD processes to enrich the plasma with SiO_2 and promote the coating. Hence, it relates to numerous applications.[42] A low HMDSO proportion in the Ar/O_2/HMDSO mixture is required to obtain a higher quality SiO_2 film, typically a few 100 ppm of HMDSO.[43] The method used in this work has the advantage of being able to produce a core shell in record time and had almost no secondary product resulting from chemical reaction because it is in the gaseous phase compared to chemical techniques like sol-gel, Stöber, and hetero-coagulation, with maximum 1 h vs 1–3 days, respectively.[44–46] Another important advantage is the fact of being able to work on all surfaces and particles with different chemical compositions of deposition compared to the layer-by-layer deposition method.[47]

II. EXPERIMENTAL

A. Experimental setup

The different compartments of the experimental device, used to realize plasma treatments, are illustrated in Fig. 1. Optical emission measurements were performed with a 750 mm imaging spectrometer (Acton SP750i) equipped with an intensified charge-coupled device (ICCD) camera (Princeton Instruments, PIMAX2, 1024 × 1024 pixels with 12.8 μm pixel size). Spectra were recorded with a 2400 lines mm^{-1} grating blazed at 240 nm. The spectral resolution defined by the full width at half maximum (FWHM) was 22 pm at 309 nm, with an entrance slit of 20 μm.

The micro-torch was driven by a pulsed generator (2 kV, 2 kHz) controlled by an arbitrary function generator (Tektronix AFG3101) set in the pulse mode. Discharge voltage and current were measured with a high voltage probe (Tektronix P6015A) and a calibrated resistor, respectively, and recorded by means of a transient digitizer (Tektronix TDS3052B, 500 MHz). In this study, the frequency of the pulse mode was fixed at 200 Hz with a pulse duration of 1000 μs (duty cycle of 20%). The discharge worked in the "auto-burst" mode at a frequency of about 0.2 MHz, as it can be seen in Fig. 2. A record of both voltage and current of a single discharge is displayed in the inset of Fig. 2; for a 630 V applied voltage, maximum current was achieved in a short time of about 40 ns.

The micro-torch was a wire/cylinder configuration with an annular discharge gap of 250 μm and a length of 2 mm. The gas mixture flowed on the axis of the reactor and the plasma appeared as a needle going out of the reactor on about 12 mm length. At the outlet of the micro-torch, the gas undergoes a strong expansion into the vacuum chamber and the pressure falls from 2.2×10^4 to 2.9×10^3 Pa. The CCTO support was placed on a translational motorized XY stage, which allows to treat a surface of 15×15 mm^2. The gap between the micro-torch and the sample was set at 2.5 mm, and an example of the micro-torch plasma behavior is given in Fig. 3.

B. Experimental procedures

CCTO particles were prepared by the standard solid-state reaction starting from a stoichiometric mixture of $CaCO_3$, CuO, and TiO_2. The reagents were first placed in isopropanol and grinded by ball milling for 6 h in a three-dimensional stirrer. After drying at 80 °C, the resulting powder was heated at 950 °C for 24 h.

The dispersion of the CCTO particles was evaluated by a Malvern zetasizer using dynamic light scattering technology. They

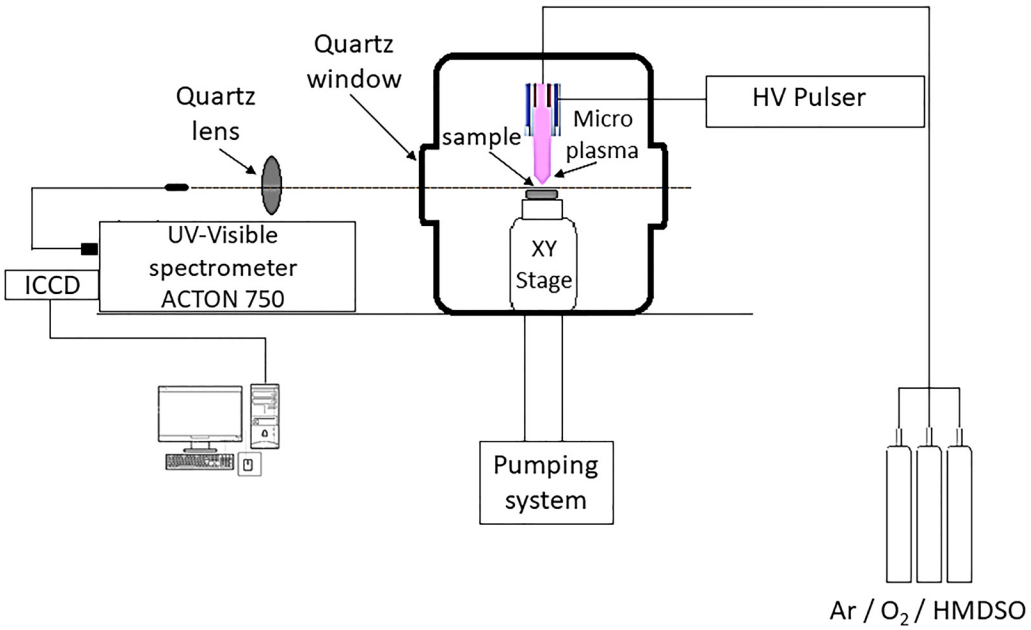

FIG. 1. Experimental setup of the plasma generator system and spectroscopic acquisition.

present a unimodal distribution with an average size of 1 μm and a dispersion of ±0.5 μm.

The CCTO fine powder was used as the "core material" for plasma "core–shell" treatment. An ink was prepared with 60% Ink Vehicle (Fuel Cells Materials) and 40% pure CCTO powder. The resulting ink was applied by screen printing on a glass substrate for all samples and then a heat treatment is realized at 90 °C for 24 h to evaporate the ink. The plasma treatments were performed into a 21 l vacuum chamber. To realize the shell of SiO_2, the first step was the plasma cleaning of the CCTO in the reaction chamber for 15 min, with 2000 N cm^3 min^{-1} of pure argon. The second step is the deposition of SiO_2 on the grains of CCTO by dissociation of HMDSO vapor introduced in the plasma using an argon/oxygen mixture. This step is done for 30 min. During experiments, the chamber was filled with a gas mixture of argon, oxygen, and

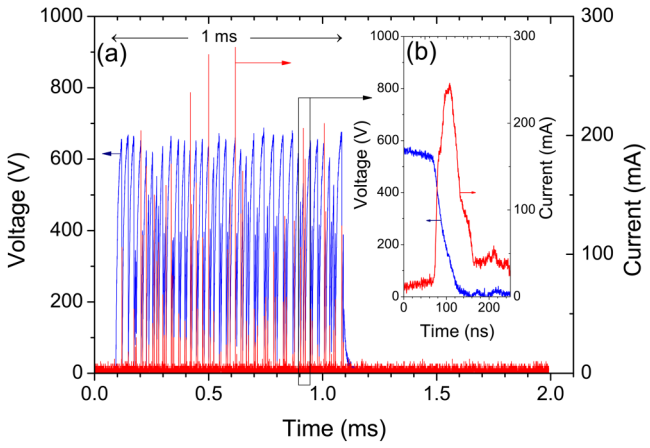

FIG. 2. (a) Details of the auto-burst mode and (b) typical time evolution of voltage and current of a single pulsed discharge for 630 V applied voltage.

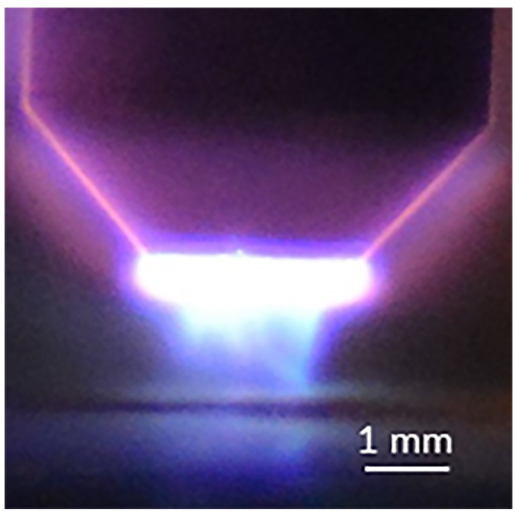

FIG. 3. Profile of the micro-torch plasma.

TABLE I. Experimental conditions of SiO_2 deposition on the CCTO grains.

	Ar flow rate ($N\,cm^3\,min^{-1}$)	O_2 flow rate ($N\,cm^3\,min^{-1}$) [mol. fraction (ppm)]	HMDSO flow rate ($mg\,h^{-1}$) [mol. fraction (ppm)]	$\frac{O_2}{HMDSO}$
Sample 1	2028 ± 12	3.00 ± 0.03 (2954 ± 57)[a]	200 ± 10 (227 ± 24)[a]	13
Sample 2	2028 ± 12	5.42 ± 0.04 (5324 ± 93)[a]	362 ± 11 (409 ± 25)[a]	13
Sample 3	2028 ± 12	7.84 ± 0.05 (7681 ± 129)[a]	523 ± 11 (589 ± 26)[a]	13

[a]With a 95% confidence level.

HMDSO vapor controlled by gas and liquid mass flow controllers at a pressure of 2.9×10^3 Pa. Resulting gas compositions used in this study were in range of 2028 $N\,cm^3\,min^{-1}$ argon/3–7.84 $N\,cm^3\,min^{-1}$ oxygen/200–523 $mg\,h^{-1}$ HMDSO. Three samples (noted samples 1–3) were selected as low, intermediate, and high HMDSO concentrations. These experimental conditions are resumed in Table I for the three samples; in addition, molecular fractions of O_2 and HMDSO were specified (mol. fraction in ppm). Spectroscopic investigations were carried out with the set of compositions: $Ar/O_2/HMDSO = 2028\ N\,cm^3\,min^{-1}/7.84\ N\,cm^3\,min^{-1}/523\ mg\,h^{-1}$, respectively. Optionally, nitrogen was introduced in very weak quantities ($4\ N\,cm^3\,min^{-1}$ or 0.2%) in the mixture for spectroscopic investigations in order to estimate the vibrational and electronic temperatures of the plasma from N_2^* and N_2^+ emissions.

The choice of the experimental conditions is based on, first, keeping the stoichiometric molecular ratio of O_2/HMDSO at 13, in order to have a complete oxidation of HMDSO to SiO_2, CO_2, and water vapor.[48] Second, the silicon dioxide concentration in the plasma increases when HMDSO and O_2 amounts are increased together.[49]

C. Characterizations after plasma treatment

The CCTO and CCTO@SiO_2 samples were characterized by room-temperature X-ray diffraction using a Bruker D8 Advance diffractometer (θ–θ) with Cu K_α radiation ($\lambda = 1.5418$ Å). The powder patterns were measured in the angular range of $20° < 2\theta < 80°$ by step of 0.02°. The morphology and the size of CCTO@SiO_2 particles were acquired by transmission electron microscopy (JEOL 2100F) operated at 200 kV and equipped with an energy dispersive spectroscopy analyzer and with scanning transmission electron microscopy (STEM). Samples for TEM, EDS, and EDS mapping measurements were prepared by crushing the crystallites in ethanol. The small flakes were deposited on a holey carbon film supported by a nickel grid. The microstructure of all samples was investigated also by MESU 1644—HR JEOL scanning electron microscopy equipped with an EDS detector.

III. RESULTS AND DISCUSSION

A. Spectroscopic investigations

Emission of plasma was investigated in the UV-visible range. The main atomic species observed in Ar/O_2/HMDSO mixtures were Si I, C I, Ar I, and O I. The molecular species identified were the ro-vibrational bands of SiO ($A^1\Pi$-$X^1\Sigma^+$) $\Delta v = v' - v'' = 0, -1$ from 234 to 250 nm. These emissions are very well identified by the position of their band heads calculated in Table II and presented in the spectrum of Fig. 4. In addition, OH° ($A^2\Sigma^+$-$X^2\Pi_i$) (0,0) at 309 nm, CH ($B^2\Sigma$-$X^2\Pi$) (0,0) at 390 nm and CH ($A^2\Delta$-$X^2\Pi$) (0,0) at 430 nm and the C_2 Swan band ($d^3\Pi_g$-$a^3\Pi_u$) (0,0) at 516.5 nm were also observed. With N_2 addition in the mixture, the N_2 second positive ($C^3\Pi_u$-$B^3\Pi_g$) $\Delta v = -2$ from 365 to 385 nm and CN ($B^2\Sigma^+$-$X^2\Sigma^+$) $\Delta v = 0$ at 388 nm and the N_2^+ second negative ($B^2\Sigma_u^+$-$X^2\Sigma_g^+$) (0,0) at 391.4 nm were detected. The presence of atomic and diatomic species derived from the HMDSO molecules demonstrates the strong dissociation power of this type of plasma.

The three ro-vibrational bands OH° ($A^2\Sigma^+$-$X^2\Pi_i$) (0,0) at 309 nm, CH ($B^2\Sigma$-$X^2\Pi$) (0,0) at 390 nm, and CH ($A^2\Delta$-$X^2\Pi$) (0,0) at 430 nm were used as thermometer species, in order to estimate the rotational temperature of the plasma. The rotational temperature was estimated individually for the three thermometers from adjustments of synthetic spectra, built from the LIFBASE code,[50] on experimental one integrated on the whole discharge. The best adjustment was $Trot = 300 \pm 10$ K. This result shows that this microplasma produces very non-Local Thermodynamic Equilibrium (non-LTE) or cold plasmas. The rotational temperature was estimated for different applied voltages. No change in rotational temperature was detected in the explored range voltage, i.e., 600–1800 V. An example is shown in Fig. 5.

Vibrational temperature was estimated from nitrogen molecules, which were introduced in very week quantities ($4\ N\,cm^3\,min^{-1}$ or 0.2%) by means of a mass flow controller in Ar/O_2/HMDSO mixtures. The vibrational temperature of molecular

TABLE II. Calculated vibrational band heads of the first vibrational states of SiO ($A^1\Pi$-$X^1\Sigma^+$).[51]

v''	$v' = 0$	$v' = 1$	$v' = 2$	$v' = 3$	$v' = 4$	$v' = 5$
0	234.47[a]	229.94	225.65	221.60	217.71	214.04
1	241.43[a]	236.63[a]	232.09	227.79	223.70	219.83
2	248.74[a]	243.65[a]	238.84[a]	234.28[a]	229.97	225.87
3	256.43	251.03	245.92[a]	241.10	236.53[a]	232.20
4	264.53	258.78	253.36	248.24[a]	243.40[a]	238.82
5	273.07	266.95	261.18	255.75	250.61	245.76[a]

[a]Observed bands in the 234–250 nm spectral range.

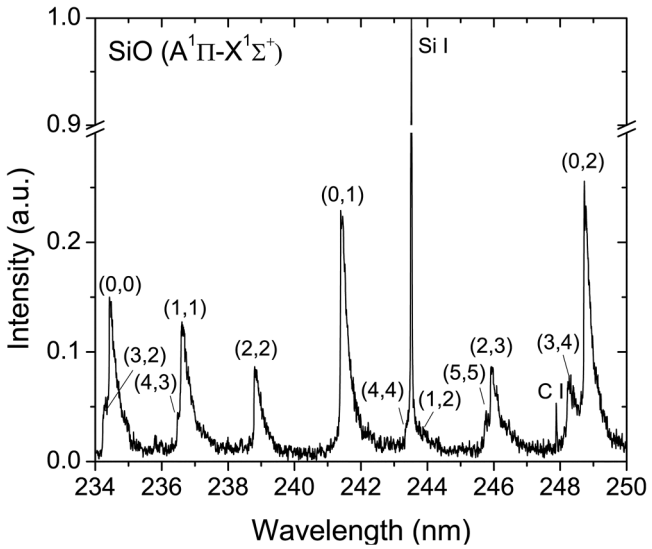

FIG. 4. Experimental spectrum of vibrational bands of SiO ($A^1\Pi$-$X^1\Sigma^+$), for a mixture (Ar/O_2/HMDSO) = (sample 3), with 1000 V applied voltage. The Si I line observed at 243.515 nm corresponds to the transition $3d^1\ D^0$–$3p^2\ ^1D$.[52]

nitrogen can be estimated from the shape of the second positive system of the nitrogen emission spectrum that corresponds to N_2 ($C^3\Pi_u$-$B^3\Pi_g$) (v′, v″) vibrational transitions.[53] In order to avoid an intensity correction of experimental spectra, we restricted the spectral range at $\Delta v = v' - v'' = -2$ between 365 and 382 nm, including the (3,5), (2,4), (1,3), and (0,2) vibrational bands. The vibrational temperature was estimated using the Boltzmann plot method described by Britun *et al.*, based on the ratio of the band heads.[54]

The vibrational excitation presents a great importance in plasma chemistry because it represents an energy storage available to initiate the chemical reaction in plasma.[55] We observe a strong enhancement of vibrational temperature with applied voltage as seen in Fig. 6, which suggests a good capacity of this plasma to generate chemical active species.

In addition, CN ($B^2\Sigma^+$-$X^2\Sigma^+$) (0,0) and (1,1) molecular emissions were observed at about 388 nm in Ar/O_2/HMDSO/N_2 mixtures. This type of spectra was interesting because it allows us to determine both Trot and Tvib on the same record. Spectra were well fitted by values of Trot and Tvib estimated above, as it can be seen in Fig. 7 for two applied voltages, which confirm these values.

Electronic temperature can be estimated from a method described by Britun *et al.*, based on the spectral band head ratio between the band head of N_2^+ second negative ($B^2\Sigma_u^+$-$X^2\Sigma_g^+$) (0,0) at 391.4 nm and the band head of N_2 second positive ($C^3\Pi_u$-$B^3\Pi_g$) (2,5) at 394.3 nm.[54] An imperative condition to be respected is that the concerned radiative species must be directly excited by electronic collisions from the ground state of N_2. This condition is not satisfied in the case of plasmas based on Ar/N_2 mixtures because of the very efficient resonant excitation transfer of N_2 from Ar metastable, which represents a non-negligible indirect channel of N_2 ($C^3\Pi_u$) production. Therefore, we have estimated the electronic temperature from a pure N_2 plasma at a flow rate of 2000 N cm^3 min^{-1}. Any variation of the electronic temperature as a function of the applied voltage was observed. The mean estimated value was Te = 5.3 ± 0.2 eV.

B. Structure and microstructure analysis

The X-ray diffraction of the CCTO powder calcined at 950 °C during 24 h and CCTO coated by SiO_2 (sample 3), are illustrated in

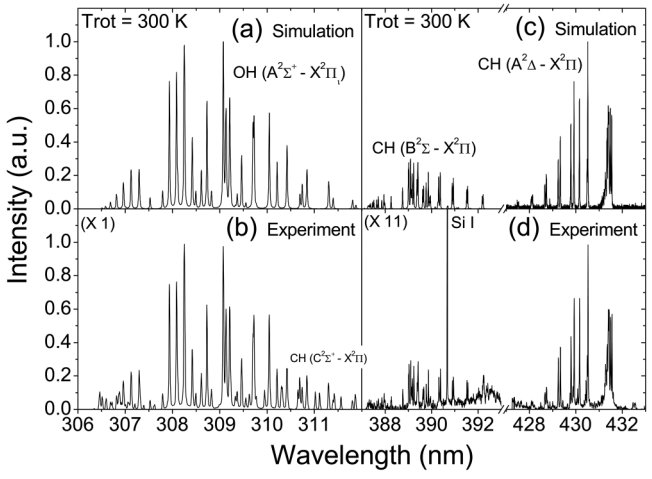

FIG. 5. Spectra of OH° ($A^2\Sigma^+$-$X^2\Pi_i$), CH ($B^2\Sigma$-$X^2\Pi$), and CH ($A^2\Delta$-$X^2\Pi$), (a) and (c) LIFBASE simulated spectra, and (b) and (d) experimental spectra ($\Delta\lambda_{app}$ = 22 pm, entrance slit = 20 μm), for a mixture (Ar/O_2/HMDSO) = (sample 3), with 1000 V applied voltage. The Si I line observed at 390.552 nm corresponds to the transition $3p4s\ 1P^0$–$3p^2\ ^1S$.[52]

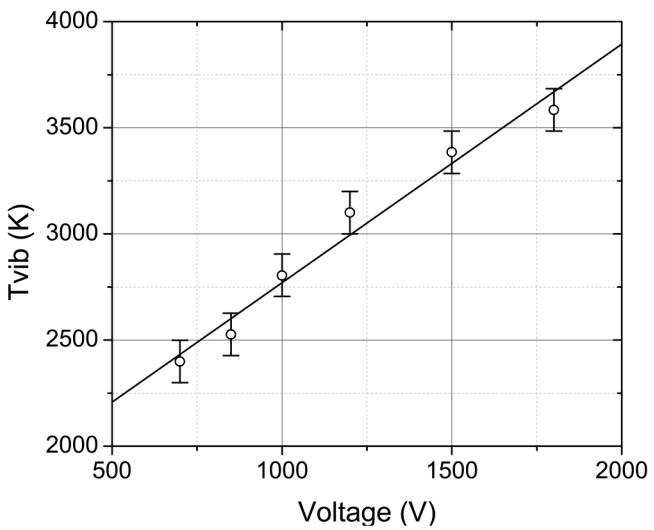

FIG. 6. Estimated vibrational temperature as a function of the applied voltage for (Ar/O_2/HMDSO/N_2) = (sample 3) + 4 N cm^3 min^{-1} of N_2.

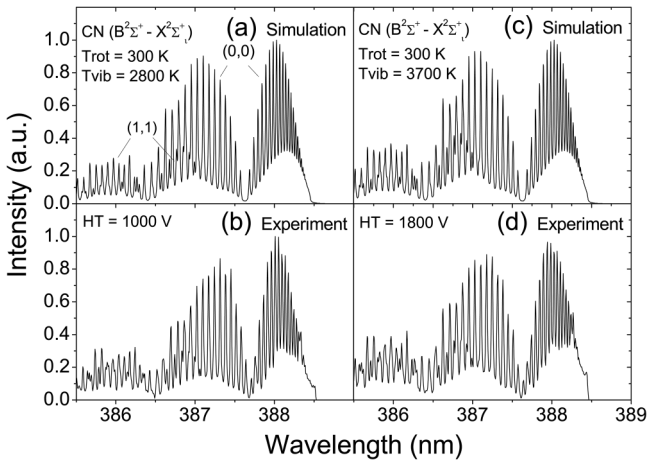

FIG. 7. Spectra of CN ($B^2\Sigma^+$-$X^2\Sigma^+$) (a) and (c) LIFBASE simulated spectra and (b) and (d) experimental spectra ($\Delta\lambda_{app}$ = 22 pm), for (Ar/O_2/HMDSO/N_2) = (sample 3) + 4 N cm^3 min^{-1} of N_2, for 1000 and 1800 V applied voltage, respectively.

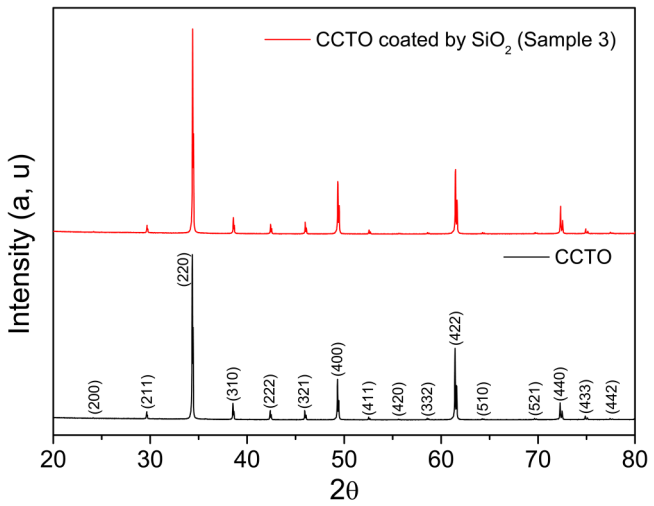

FIG. 8. X-ray diffraction patterns of the CCTO powder calcined at 950 °C during 24 h and CCTO coated by SiO_2 (sample 3).

Fig. 8. Corresponding to the PDF number of ICDD 04-010-5727, the XRD analysis confirms that all peaks match with those of the CCTO pure phase, and no supplementary peaks are observed. SiO_2 peaks do not appear probably because the shell is amorphous. The CCTO compound crystallizes in a cubic structure with a cell parameter a = 7.393 Å and space group Im-3m.

According to the EDS analysis of the three samples, shown in Fig. 9, the presence of Si element is observed. In the table of Fig 9, the weight percentage of the Si element increases from 9.28% to 17.96% when the O_2 and HMDSO concentrations increase.

SiO_2 shell formed by plasma deposition on the CCTO grains was analyzed by TEM and EDS mapping. As can be seen in Fig. 10, the SiO_2 shell and the CCTO core are distinguishable as bright and dark regions, respectively, due to the differences in density between the two phases. Figure 10(a) corresponds to sample 1 and Fig. 10(b) to sample 2. For both samples, the CCTO grains are not well coated. So, the shell is not homogenous when we use these chemical conditions. As we can see in Fig. 10(a), there are only some areas coated with SiO_2 (white circles). In these two cases, it is probably due to the quantity of SiO_2 resulting from the dissociation of HMDSO, which is insufficient for coating all the grains of CCTO and forms a homogeneous shell. In Fig. 10(b), CCTO is well crystallized, as it is shown in the white square; the atomic arrangement can be clearly observed with white and dark dots; and this crystallization was determined

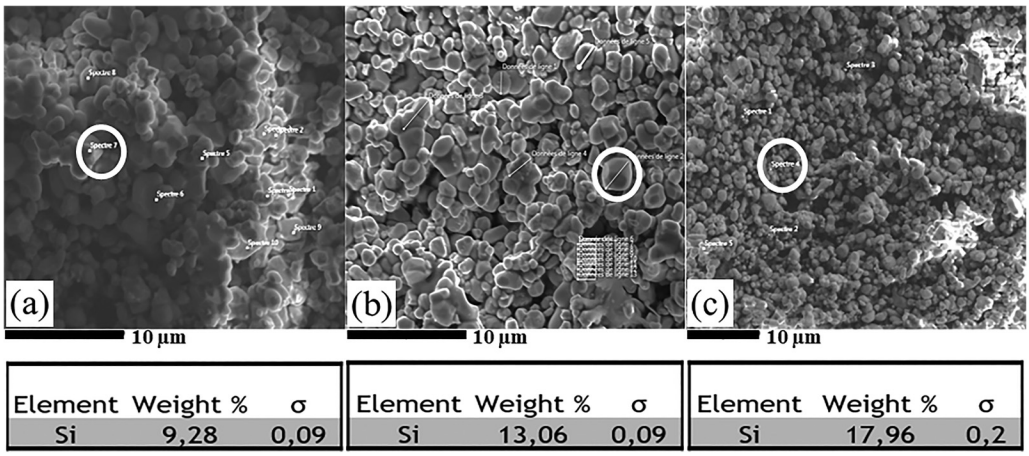

FIG. 9. EDS analysis in the white circle area of CCTO@SiO_2 for (a) sample 1, (b) sample 2, and (c) sample 3.

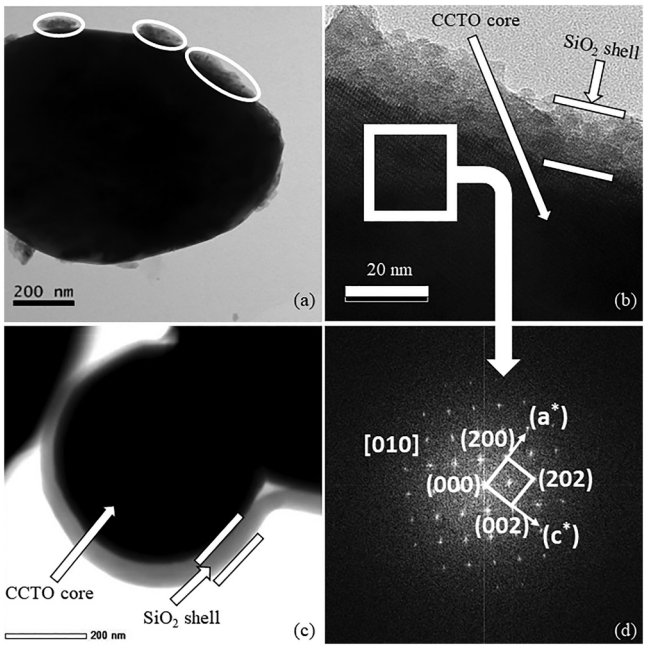

FIG. 10. TEM pictures of CCTO@SiO_2 (a) sample 1, (b) sample 2, and (c) sample 3 and (d) diffraction spots of the crystalline CCTO of the white square.

according to the diffraction spots as shown in Fig. 10(d). The first measured inter-reticular distance was 3.69 Å that corresponds to the (200) diffraction plane (3.6899 Å as it is shown in the PDF number of ICDD 04-010-5727) and gives a lattice parameter of 7.37 Å that coincides with the theoretical lattice parameter of this material. The SiO_2 shell do not show any orientation, so it is amorphous. Figure 10(c) corresponding to sample 3 shows that the increase in the concentration of oxygen and HMDSO makes the shell of SiO_2 homogenous. The whole grain of CCTO is coated. The average thickness of this shell is about 50 nm, determined with several particles based on the TEM image scale. The mapping data of principal elements present in the designated cartography zone [Fig. 10(c)] are analyzed.

The mapping of O, Si, Cu, and Ti and the superposition of these elements are shown in Fig. 11(a) and confirmed that CCTO grains are coated with Si. Figure 11(b) shows the combination of Si with a blue color and O with red one, which gives a purple color when they are overlaid. This means that there is an association between Si and O to give SiO (SiO_2), which confirms the core–shell structure.

Figure 12 shows the evolution of the shell thickness that rises with the increase in the HMDSO's amount for the same treatment time.

The shell attachment processes and the deposition mechanism remain a questionable subject. We can issue several hypotheses. Several research groups have explained that this deposition

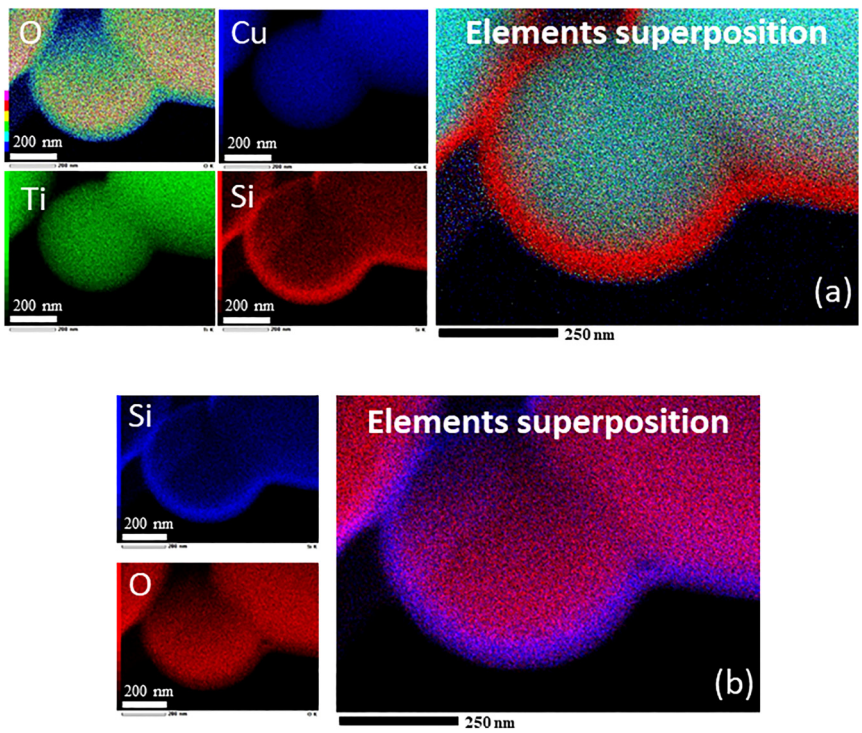

FIG. 11. EDS–TEM mapping pictures corresponding to sample 3 of elements and their superposition: (a) O, Cu, Ti, and Si; (b) Si and O.

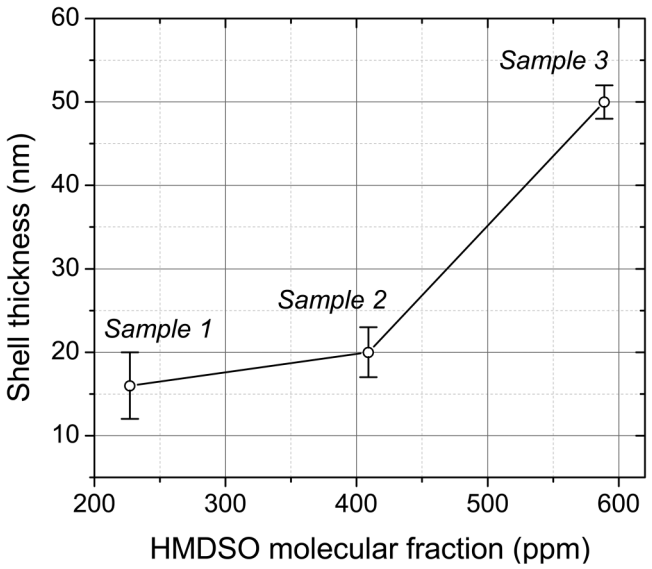

FIG. 12. Shell thickness depending on the HMDSO molecular fraction.

mechanism depends on the way in which the HMDSO is fragmented. In fact depending on the used energy, there can be several mechanisms of dissociation of the HMDSO molecule to $(CH_3)_2$—Si—O, $(CH_3)_3$—Si—O, Si—O—Si, Si—O, CH_2, Si, and CH_2—CH_2—O,[56–59] which will influence the quality and the chemical composition of the deposit.[54] The insertion of oxygen into the plasma promotes the formation of volatile groups in the gas phase, such as CO_2, CO, and COH_2. This allows a very good quality deposit with less carbon groups. It could explain the high quality of our shell, as we see in Fig. 10 of the TEM image.[60,61] During the plasma treatment, spectroscopic investigations prove that the HMDSO molecule is completely dissociated (Si, C, CH, O, and SiO). Experiments carried out without oxygen in the mixture showed the absence of SiO emissions in the plasma phase and the absence of deposit on the CCTO.

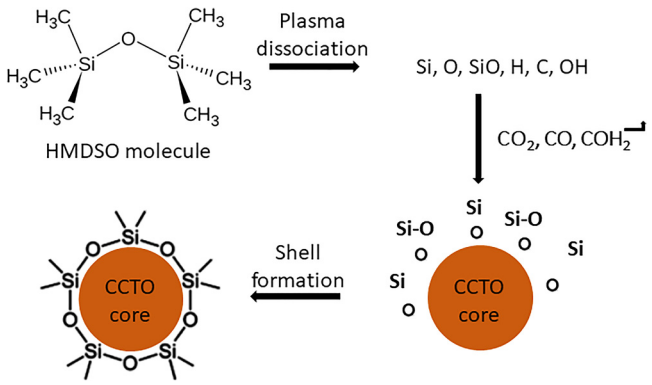

FIG. 13. Shell formation process on the CCTO grains.

This confirms that the formation of SiO_X is mainly due to the oxygen atoms issued from oxygen molecules' dissociation added during experiments rather than oxygen atoms present in the HMDSO molecules. Our hypothesis is that the oxygen, silicon, and silicon oxide surround the CCTO's grains. Their association allows us to form silicon dioxide. As a result, the CCTO grains are found trapped in a shell, as shown in Fig. 13. This process can explain the formation of the shell in this experiment.

IV. CONCLUDING REMARKS

The non-equilibrium plasma deposition described in this work is advantageous over other methods reported in the recent literature[17,19] owing to its rapidness, its dry character, and the homogeneous shell. The present system for the CCTO@SiO_2 synthesis is based on micro-plasma of an oxidizing gas mixture containing HMDSO precursor vapor, which is introduced in the plasma using a carrier gas flow. The metalorganic precursor (HMDSO) is dissociated in the plasma and the resulting SiOx nucleates to the surface of CCTO particles. This system facilitated the generation of uniform "core–shell" grains CCTO@SiO_2 with the SiO_2 shell thickness of 50 ± 2 nm.

Results of temperature measurements presented in this study, i.e., Trot < Tvib ≪ Te, confirm the non-LTE character of this micro-plasma. These types of plasmas are, therefore, well adapted to chemical treatments by efficiently generating chemically active species by electronic collisions without overheating the whole gas. A proof of this is the dissociation of HMDSO molecules into atomic and diatomic species.

The successful synthesis of the CCTO core and the SiO_2 shell was demonstrated using SEM, EDS, and TEM. Whatever the concentration of HMDSO in the plasma, the TEM images confirm a deposit of SiO_2 on the CCTO grain. The homogeneity was better for the set of values: O_2/HMDSO = 7681/589 ppm, respectively, with a shell thickness of 50 nm. According to the TEM images and weight percentage given by the EDS analysis, we can conclude that the increase in HMDSO quantity improves the quality and homogeneity of the coating. However, in this work, it was not possible to realize electrical measurements in order to determine the permittivity and the dielectric losses because of the low quantity of the core–shell powder obtained. In principle, the strategy and objective of our study offer a new opportunity to quickly synthetize homogenous core–shell materials with a plasma technique.

DATA AVAILABILITY

The data that support the findings of this study are available from the corresponding author upon reasonable request.

REFERENCES

[1]C. C. Homes, T. Vogt, S. M. Shapiro, S. Wakimoto, and A. P. Ramirez, Science **293**, 673 (2001).
[2]M. T. Buscaglia, M. Viviani, V. Buscaglia, L. Mitoseriu, A. Testino, P. Nanni, Z. Zhao, M. Nygren, C. Harnagea, D. Piazza, and C. Galassi, Phys. Rev. B **73**, 064114 (2006).
[3]A. M. Bratkovsky and A. P. Levanyuk, Phys. Rev. Lett. **94**, 107601 (2005).
[4]H. Han, C. Voisin, S. Guillemet-Fritsch, P. Dufour, C. Tenailleau, C. Turner, and J. C. Nino, J. Appl. Phys. **113**, 024102 (2013).

[5]P. Lunkenheimer, S. Krohns, S. Riegg, S. G. Ebbinghaus, A. Reller, and A. Loidl, Eur. Phys. J. Spec. Top. **180**, 61 (2009).
[6]M. A. Subramanian, D. Li, N. Duan, B. A. Reisner, and A. W. Sleight, J. Solid State Chem. **151**, 323 (2000).
[7]A. P. Ramirez, M. A. Subramanian, M. Gardel, G. Blumberg, D. Li, T. Vogt, and S. M. Shapiro, Solid State Commun. **115**, 217 (2000).
[8]M. A. Subramanian and A. W. Sleight, Solid State Sci. **4**, 347 (2002).
[9]V. Brizé, G. Gruener, J. Wolfman, K. Fatyeyeva, M. Tabellout, M. Gervais, and F. Gervais, Mater. Sci. Eng. B **129**, 135 (2006).
[10]R. Bodeux, M. Gervais, J. Wolfman, C. Autret-Lambert, G. Liu, and F. Gervais, Thin Solid Films **520**, 2632 (2012).
[11]A. P. Litvinchuk, C. L. Chen, N. Kolev, V. N. Popov, V. G. Hadjiev, M. N. Iliev, R. P. Bontchev, and A. J. Jacobson, Phys. Status Solidi A **195**, 453 (2003).
[12]P. Lunkenheimer, V. Bobnar, A. V. Pronin, A. I. Ritus, A. A. Volkov, and A. Loid, Phys. Rev. B **66**, 52105 (2002).
[13]D. C. Sinclair, T. B. Adams, F. D. Morrison, and A. R. West, Appl. Phys. Lett. **80**, 2153 (2002).
[14]T. B. Adams, D. C. Sinclair, and A. R. West, Phys. Rev. B **73**, 094124 (2006).
[15]S. De Almeida-Didry, C. Autret, A. Lucas, C. Honstettre, F. Pacreau, and F. Gervais, J. Eur. Ceram. Soc. **34**, 3649 (2014).
[16]C. Autret, S. De Almeida, and F. Gervais, *Promising Trends in Materials for Ceramic Capacitors* (LAP Lambert Academic Publishing Inc., 2020), ISBN:978-620-3-04208-5.
[17]S. De Almeida-Didry, M. M. Nomel, C. Autret, C. Honstettre, A. Lucas, F. Pacreau, and F. Gervais, J. Eur. Ceram. Soc. **38**, 3182 (2018).
[18]S. De Almeida-Didry, C. Autret, A. Lucas, F. Pacreau, and F. Gervais, Solid State Sci. **96**, 105943 (2019).
[19]S. De Almeida-Didry, S. Merad, C. Autret-Lambert, M. M. Nomel, A. Lucas, and F. Gervais, Solid State Sci. **109**, 106431 (2020).
[20]S. Li, X. Dang, X. Yu, G. Abbas, Q. Zhang, and L. Cao, Chem. Eng. J. **388**, 124275 (2020).
[21]M. Schiavon, V. Torretta, A. Casazza, and M. Ragazzi, Water Air Soil Pollut. **228**, 388 (2017).
[22]J. Van Durme, J. Dewulf, C. Leys, and H. Van Langenhove, Appl. Catal. B **78**, 324 (2008).
[23]A. M. Vandenbroucke, R. Morent, N. De Geyter, and C. Leys, J. Hazard. Mater. **195**, 30 (2011).
[24]F. L. Tabares and I. Junkar, Molecules **26**, 1903 (2021).
[25]S. K. Pankaj, Z. Wan, and K. M. Keener, Foods **7**, 4 (2018).
[26]M. Laroussi, IEEE Trans. Plasma Sci. **30**, 1409 (2002).
[27]M. Laroussi and T. Akan, Plasma Process Polym. **4**, 777 (2007).
[28]M. Moreau, N. Orange, and M. G. J. Feuilloley, Biotechnol. Adv. **26**, 610 (2008).
[29]B. Surowsky, O. Schlüter, and D. Knorr, Food Eng. Rev. **7**, 82 (2015).
[30]P. Dimitrakellis and E. Gogolides, Adv. Colloid Interface Sci. **254**, 1 (2018).
[31]U. Kogelschatz, Plasma Chem. Plasma Process. **23**, 1 (2003).
[32]P. R. McCurdy, C. I. Butoi, K. L. Williams, and E. R. Fisher, J. Phys. Chem. B **103**, 6919 (1999).
[33]R. Dorai and M. J. Kushner, J. Phys. D: Appl. Phys. **36**, 666 (2003).
[34]A. P. Papadakis, S. Rossides, and A. C. Metaxas, Open Appl. Phys. J. **4**, 45 (2011).
[35]T. Belmonte, G. Arnoult, G. Henrion, and T. Gries, J. Phys. D: Appl. Phys. **44**, 363001 (2011).
[36]M. J. Kushner, J. Phys. D: Appl. Phys. **38**, 1633 (2005).
[37]K. H. Becker, K. H. Schoenbach, and J. G. Eden, J. Phys. D: Appl. Phys. **39**, R55 (2006).
[38]R. Foest, M. Schmidt, and K. Becker, Int. J. Mass Spectrom. **248**, 87 (2006).
[39]L. Martinu and D. Poitras, J. Vac. Sci. Technol. A **18**, 2619 (2000).
[40]M. Meyyappan, L. Delzeit, A. Cassell, and D. Hash, Plasma Sources Sci. Technol. **12**, 205 (2003).
[41]A. Gangele, C. S. Sharma, and A. K. Pandey, J. Nanosci. Nanotechnol. **17**, 2256 (2017).
[42]F. Massines, N. Gherardi, A. Fornelli, and S. Martin, Surf. Coat. Technol. **200**, 1855 (2005).
[43]A. Bellel, S. Sahli, Z. Ziari, P. Raynaud, Y. Segui, and D. Escaich, Surf. Coat. Technol. **201**, 129 (2006).
[44]H. Peng, R. Liang, and J. Qiu, Biosens. Bioelectron. **26**, 3005 (2011).
[45]W. Stöber, A. Fink, and E. Bohn, J. Colloid Interface Sci. **26**, 62 (1968).
[46]P. Garcia-Perez, C. Pagnoux, F. Rossignol, and J. F. Baumard, Colloids Surf. A Physicochem. Eng. Aspects **281**, 58 (2006).
[47]X. Zhang, H. Chen, and H. Zhang, Chem. Commun. **14**, 1395 (2007).
[48]R. Barni, S. Zanini, and C. Riccardi, Adv. Phys. Chem. **2012**, 1.
[49]C. Vautrin-Ul, C. Boisse-Laporte, N. Benissad, A. Chausse, P. Leprince, and R. Messina, Prog. Org. Coat. **38**, 9 (2000).
[50]J. Luque and D. R. Crosley, Lifbase: *Database and spectral simulation program* (version 2.1.1). SRI International Report MP 99-009 (1999).
[51]O. Motret, F. Coursimault, R. Viladrosa, and J.-M. Pouvesle, J. Phys. D: Appl. Phys. **36**, 2060 (2003).
[52]A. Kramida and Y. Ralchenko, J. Reader and NIST ASD Team (2020). NIST Atomic Spectra Database (ver. 5.8) (Online) see https://physics.nist.gov/asd (2021 September 16), National Institute of Standards and Technology, Gaithersburg, MD, https://doi.org/10.18434/T4W30F
[53]U. Fantz, Plasma Sources Sci. Technol. **15**, S137 (2006).
[54]N. Britun, M. Gaillard, A. Ricard, Y. M. Kim, K. S. Kim, and J. G. Han, J. Phys. D: Appl. Phys. **40**, 1022 (2007).
[55]A. Fridman and L. A. Kennedy, *Plasma Physics and Engineering* (Taylor & Francis, 2004).
[56]N. E. Blanchard, B. Hanselmann, J. Drosten, M. Heuberger, and D. Hegemann, Plasma Process. Polym. **12**, 32 (2015).
[57]Y. Y. Ji, Y. C. Hong, S. H. Lee, S. D. Kim, and S. S. Kim, Surf. Coat. Technol. **202**, 5663 (2008).
[58]F. Fracassi, R. d'Agostino, and P. Favia, J. Electrochem. Soc. **139**, 2636 (1992).
[59]M. Creatore, F. Palumbo, and R. d'Agostino, Plasmas Polym. **7**, 291 (2002).
[60]F. Fracassi, R. d'Agostino, F. Fanelli, A. Fornelli, and F. Palumbo, Plasmas Polym. **8**, 259 (2003).
[61]D. Magni, C. Deschenaux, C. Hollenstein, A. Creatore, and P. Fayet, J. Phys. D: Appl. Phys. **34**, 87 (2001).